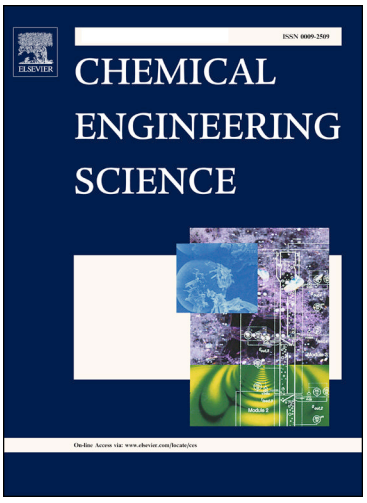

Estimating the hindered-settling flux function from a batch test in a cone

Raimund Bürger, Julio Careaga, Stefan Diehl, Ryan Merckel, Jesús Zambrano

PII: S0009-2509(18)30499-8
DOI: https://doi.org/10.1016/j.ces.2018.07.029
Reference: CES 14383

To appear in: *Chemical Engineering Science*

Received Date: 22 November 2017
Accepted Date: 13 July 2018

Please cite this article as: R. Bürger, J. Careaga, S. Diehl, R. Merckel, J. Zambrano, Estimating the hindered-settling flux function from a batch test in a cone, *Chemical Engineering Science* (2018), doi: https://doi.org/10.1016/j.ces.2018.07.029

Estimating the hindered-settling flux function from a batch test in a cone

Raimund Bürger[a], Julio Careaga[b,*], Stefan Diehl[b], Ryan Merckel[c], Jesús Zambrano[d]

[a] *CI²MA and Departamento de Ingeniería Matemática, Universidad de Concepción, Concepción, Chile*
[b] *Centre for Mathematical Sciences, Lund University, P.O. Box 118, S-221 00 Lund, Sweden*
[c] *Department of Chemical Engineering, University of Pretoria, South Africa*
[d] *School of Business, Society and Engineering, Mälardalen University, Västerås, Sweden*

Abstract

The hindered-settling velocity function for the modelling, simulation and control of secondary settling tanks can be determined from batch tests. The conventional method is to measure the velocity of the descending sludge-supernatant interface (sludge blanket) as the change in height over time in a vessel with constant cross-sectional area. Each such experiment provides one point on the flux curve since, under idealizing assumptions (monodisperse suspension, no wall-effects), the concentration of sludge remains constant just below the sludge blanket until some wave from the bottom reaches it. A newly developed method of estimation, based on the theory of nonlinear hyperbolic partial differential equations, is applied to both synthetic and experimental data. The method demonstrates that a substantial portion of the flux function may be estimated from a single batch test in a conical vessel. The new method takes into consideration that during an ideal settling experiment in a cone, the concentration just below the sludge blanket increases with time since the mass of suspended solids occupy a reduced volume over time.

Keywords: identification, inverse problem, partial differential equation, sedimentation

*Corresponding author

Email addresses: rburger@ing-mat.udec.cl (Raimund Bürger), julio.careaga@math.lth.se (Julio Careaga), stefan.diehl@math.lth.se (Stefan Diehl), U26015383@tuks.co.za (Ryan Merckel), jesus.zambrano@mdh.se (Jesús Zambrano)

1. Introduction

The simulation and control of sedimentation in primary and secondary settling tanks in water resource recovery facilities relies on calibrated models. The time variation of the physical properties of biological sludge makes it necessary to recalibrate repeatedly. This limitation calls for efficient methods that are based on simple experiments. Calibration of a model requires solving an inverse problem, which means that given the initial data and the solution of a differential equation, unknown material-specific model parameters or even entire constitutive functions appearing in the equation are determined. In the present paper, we use observations from an experiment as inputs to the inverse problem to estimate the unknown flux function of a partial differential equation (PDE). This is what we call a method of estimation. The unknown batch-settling flux function is the product of the hindered-settling velocity and concentration, and it appears in any model of sedimentation in any dimension.

Inverse problems are sensitive to measurement errors and often ill-posed; different sets of parameter values may produce the same output. In practice, measured data are compared to the outputs of the model. The most common way is a perform a batch test of an initially homogeneous suspension in a cylindrical vessel (Torfs et al., 2016b) and measure the position of the sludge blanket level (SBL) as a function of time. After a possible short induction period, when stirring turbulence has ceased and some flocculation may have occurred, the SBL descends at constant velocity corresponding to a straight line in a height-versus-time plot. This gives the hindered-settling velocity for the concentration below the SBL, which is equal to the initial concentration unless this is so high that compression is present already from the start. Such standard tests are used for fitting parameters of some appropriate settling-velocity function, the most common being the exponential function by Vesilind (1968) or the modified function by Tak´acs et al. (1991); see e.g. (Vesilind, 1968; Ozinsky and Ekama, 1995; Vanderhasselt and Vanrolleghem, 2000; Zhang et al., 2006; Iritani et al., 2009; Mancell-Egala et al., 2016). Compared to the many publications on sedimentation in a cylindrical vessel, very few exist in the case of a conical vessel (White and Verdone, 2000).

Ramin et al. (2014) report batch experiments with measurements both of the SBL and the bottom concentration, which gives valuable information on how to estimate not only the settling flux, but also the compression function. They obtained good agreement with data with a model consisting of exponential functions for the hindered-settling flux and a power-law function for the compression function. Unfortunately, the model parameters depend on the initial concentration C_0, which makes the model difficult to use fo r continuous sedimentation. The difficulty of finding a compression function that is independent of the batch test itself is a problem not yet resolved; see also (De Clercq et al., 2005; Diehl, 2015) and this is out of the scope of this article.

More advanced methods of measuring batch tests giving accurate information on the concentration as function of location and time also below the SBL (De Clercq et al., 2005; Locatelli et al., 2015; Fran¸cois et al., 2016) provide much more information on hindered settling at intermediate concentrations and compression at higher concentrations. These accurate findings have led to the conclusion that the common hindered-settling function by Vesilind is not satisfactory when compression is taken into account (De Clercq et al., 2005; Diehl, 2015; Torfs et al., 2017). Although these works recommend a hindered-settling velocity function of the power-law type for activated sludge, it is difficult to draw any definite conclusion for all types of sludges. Improved estimation methods that do not rely on any predefined functional relationship of the settling velocity function, or equivalently, the settling flux function, are therefore required. One such example is the graphical method of Kynch (1952), by which a convex part of the flux function can be estimated from one batch test. Kynch's graphical method was later expressed by means of parametric and explicit formulae by Diehl (2007), who also presented a new settling experiment to identify the concave part of the flux for lower concentrations. These methods were developed further by Bu¨rger and Diehl (2013). A drawback of that new settling experiment is that a special equipment is needed. Similar results on the estimation of a portion of the flux function from a conventional batch test without assuming any particular form and by utilizing piecewise rational functions were presented by Grassia et al. (2011); see also references therein.

Whatever the batch experiment, the procedure for estimating the flux during every-day

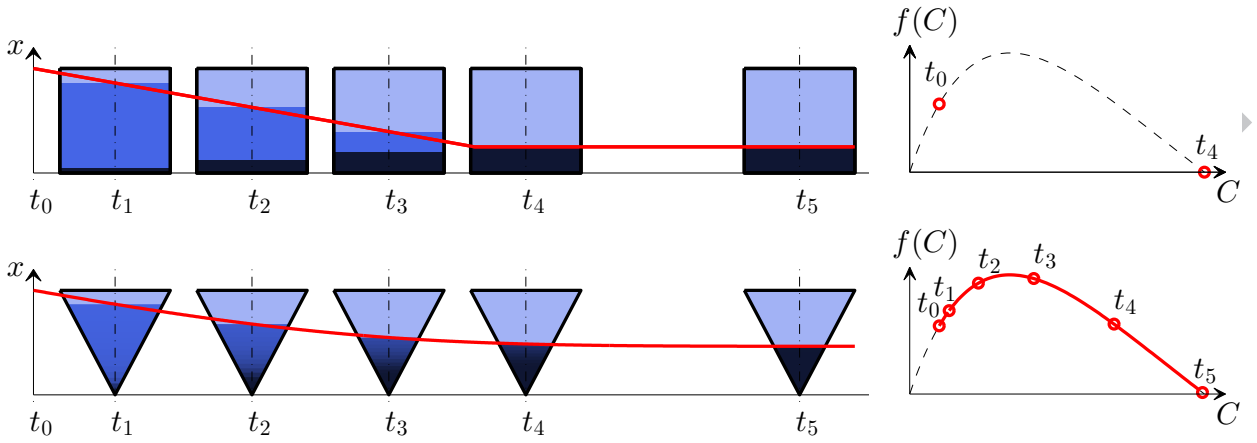

Figure 1: (from Bürger et al., 2018) Conventional method (above) and new method (below) of estimating the settling flux function. The blue scale in the vessels corresponds to concentrations obtained by numerical simulation of the model PDE.

operation means that the SBL is measured as a function of time. A novel method by using an off-the-shelf camera, image analysis and a multivariate shape-constrained spline model for the automatic registration of the SBL is presented by Derlon et al. (2017). Their method could preferably be used also for batch settling in a cone, not only for automation, but also where accurate measurements are needed.

We here validate a novel method of estimation, which under idealizing conditions requires the measurement of the SBL as a function of time during only one batch-settling test in a conical vessel. The method (solution of the inverse problem) for vessels of different shapes was derived mathematically by Burger et al. (2018). This in turn uses the knowledge of the exact solution by the method of characteristics for first-order hyperbolic PDE presented by B¨urger et al. (2017a), who were inspired by the work of Anestis (1981). Unfortunately, this could only be done under the restricted assumption that only hindered settling is present. The new method utilizes that under idealizing assumptions (monodisperse suspension, homogeneous concentration at each height, no wall effects, etc.), the concentration just below the SBL increases with time already from the start in a conical vessel, whereas it is constant (for a while) in a cylindrical vessel (Figure 1).

The purpose of this work is to validate the new method on experimental data with activated sludge and conclude by means of synthetic data that the method can be applied to low concentrations below which there is no compression.

2. Theoretical method

Batch sedimentation in a vessel with varying cross-sectional area $A(x)$, where x is the height measured from the bottom of the vessel, can be modelled by the following conservation of mass PDE, where t is time and $C = C(x,t)$ is the solids concentration:

$$A(x)\frac{\partial C}{\partial t} = \frac{\partial}{\partial x}\left(A(x)\right) f(C) + d(C)\frac{\partial C}{\partial x} \quad . \tag{1}$$

Here, $f(C) = Cv_{\mathrm{h}}(C)$ is the hindered-settling flux function, where $v_{\mathrm{h}}(C)$ is the hindered-settling velocity (positive downwards, i.e., in the negative x-direction). Furthermore, $d(C) = Kv_{\mathrm{h}}(C)\mathrm{d}\sigma_{\mathrm{e}}/\mathrm{d}C$ is the compression function, where K is a constant and $\sigma_{\mathrm{e}}(C)$ the effective solids stress function which is zero below a critical concentration C_{crit}, i.e., compression occurs above C_{crit}. Hence, $v_{\mathrm{h}}(C)$ appears in both terms of the PDE corresponding to hin-dered and compressive settling (B¨urger et al., 2011), and this function can also be used for modelling discrete settling (Torfs et al., 2016a).

We now describe the solution of the PDE and two methods of solution of the inverse problem of estimating (a portion of) the flux function f. In theory, both methods give the same result. Consider first the PDE solution describing the traditional batch test in a cylindrical vessel with homogeneous initial concentration C_0, where we assume $C_0 < C_{\mathrm{crit}}$. The concentration in a region below the discontinuity representing the SBL is constant C_0, the settling velocity is $v_{\mathrm{h}}(C_0)$ and one point on the flux curve can be obtained by measuring the velocity of the descending SBL (Figure 1). Another test with a different initial concentration gives another point on the curve, etc. In a downward-contracting vessel, the solution of the PDE has an increasing concentration just below the SBL discontinuity from $t = 0$. In reality, this corresponds to the fact that the particles are forced to move together when settling. The new estimation method utilizes this phenomenon and, under the assumption that no compression is present, i.e. $d(C) \equiv 0$ in (1), the flux $f(C)$ can

be estimated on the entire interval $C_0 \leqslant C \leqslant C_{\max}$, where $C_{\max}$ is the maximum packing concentration for the material (Figure 1). Assuming that no compression is present is equivalent to assuming $C_{\text{crit}} = C_{\max}$.

One advantage of this new method is that, at least in theory, only one batch experiment needs to be performed. Another advantage is that a large part of the flux function $f(C)$ is obtained without assuming any specific functional expression. As with many methods of solution of inverse problems, the proposed method is sensitive to inaccurate measurements and noise. Another insufficiency is that it can only be used before the region of compression influences the SBL, which implies that it can estimate $f(C)$ only up to some concentration below C_{crit}. We demonstrate this by the example below using synthetic data.

Theoretically, the smaller the initial concentration C_0 is, the larger the C-interval becomes for which the flux function can be estimated. The formulas we present here are valid for the most advantageous case of vessel, namely a full cone with a vertex at the bottom for the suspension to fill out, i.e., there should be no small flat bottom. Truncated cones, including other shapes of vessel, can be handled (Burger et al., 2018); however, the formulas are more involved and, more importantly, they are only valid up to a certain time point when a certain wave of concentration from the bottom reaches the SBL and this time point seems to be very difficult to establish experimentally.

Method of estimation

1. Perform a batch-settling test in a vessel such that the suspension fills out a cone with its vertex at the bottom (cf. Figure 1) and with the initial homogeneous concentration C_0. Let H be the height of the suspension surface above the bottom vertex. Collect data points $(t_j\,, x_j\,)$, $j = 1, \ldots, N$, along the descending SBL, i.e., x_j is its height at time t_j.

2. Fit a curve $x = h(t)$ to the data set (t_j, x_j), $j = 1, \ldots, N$, for example, with a least-squares method. In this work, $h(t)$ consists of several piecewise cubic polynomials, whose coefficients are obtained from the optimization problem described in AppendixA.

3. The estimated portion of the flux function is given by the following parametrization:

$$\begin{cases} C = \dfrac{C_0 H^3}{h(t)^2\,(h(t) - t h'(t))} \\ f_{\mathrm{par}}(C) = -\dfrac{C_0 H^3}{h(t)^2\,(h(t) - t h'(t))} h'(t) \end{cases} \quad \text{for} \quad 0 \leqslant t \leqslant t_N. \quad (2)$$

This gives the shape of the flux function in the interval $[C_0,\, C(t_N)]$. To obtain a full flux, the representation in the interval $[0,\, C_0]$ can be a second-order polynomial $p(C)$ satisfying $p(0) = f_{\mathrm{par}}(0) = 0$, $p(C_0) = f_{\mathrm{par}}(C_0)$ and $p'(C_0) = f_{\mathrm{p}}{}'_{\mathrm{ar}}(C_0)$ and for the interval $[C(t_N), C_{\max}]$, a straight line can be fitted.

4. An approximate and explicit representation of the flux function can be obtained by a nonlinear fit to the parametric representation f_{par} given by (2).

Comments and practical considerations

The core of the estimation method is formula (2), which was derived by B¨urger et al. (2018). It gives the exact solution of the inverse problem of estimating (a part of) the flux function f when the effective solids stress function is zero and when the data in step 1 come from the solution of PDE (1). We emphasize that the shape of the flux as a function of C is theoretically independent of the initial data C_0, despite the parametrization (2) contains C_0 explicitly. The explanation is that also $h(t)$ depends on C_0 in such a way that the entire expression is independent of C_0. This follows from the derivation by B¨urger et al. (2018). Hence, a new experiment with a different value of C_0 will only result in a change in the left endpoint of the interval of concentrations for which the flux is estimated. The results by B¨urger et al. (2018) also state that as long as any curve fitting function $h(t)$ that satisfies $h'(t) < 0$ and $h''(t) > 0$ is used, then the parametrization (2) is indeed the graph of a *function* $f_{\mathrm{par}}(C)$. The regularity of this function is of one degree less than $h(t)$. For example, $h \in C^2$ (twice continuously differentiable function) implies that $f \in C^1$.

The additional nonlinear curve fittings in steps 2 and 4 can be made in different (standard) ways with different functional expressions depending on the materials of the suspen-

sion. The final estimated flux is sensitive to the accuracy of the fit $x = h(t)$ in step 2.

Although the parametric representation of the flux function $f(C)$ in step 3 can be used in a simulation program, an explicit representation of $f(C)$ (step 4) is preferred. Many such functions have been suggested for different materials (Zeidan et al., 2003; Torfs et al., 2017).

As for preparing the experiment (step 1), a small initial concentration C_0 is preferable from a theoretical point of view since the flux $f(C)$ can only be estimated for co ncentrations above C_0. A small initial concentration will also reduce or avoid the often seen initial induction period, during which turbulence due to initial stirring ceases and some flocculation occurs. This induction period is ignored in our present method. A small C_0 has, however, practical difficulties, such as to detect the SBL.

3. Estimation using synthetic data with and without compression

We demonstrate the estimation method in Section 2 on synthetic data that are obtained by numerical simulations of a batch test in a conical vessel by the numerical method of B¨urger et al. (2017b) that handles the varying cross-sectional area down to zero. The flux function is thus known (the dashed black curve in Figure 2(c)) and the method can be evaluated with respect to its sensitivity for measurement errors and performance when compression is present. The height is set to $H = 0.383$ m (the same as in the experiments below) and the following constitutive functions are used (Diehl, 2015; Torfs et al., 2017):

$$v_{\mathrm{h}}(C) = \frac{v_0}{1 + (C/\bar{C})^n} - \frac{v_0}{1 + (C_{\max}/\bar{C})^n}, \tag{3}$$

$$\sigma_{\mathrm{e}}(C) = \begin{cases} 0 & \text{for } 0 \leqslant C \leqslant C_{\mathrm{crit}}, \\ \alpha(C - C_{\mathrm{crit}}) & \text{for } C > C_{\mathrm{crit}}, \end{cases}$$

where the following parameters were chosen to be the same as in Section 4; see Figure 6: $v_0 = 6.2153 \times 10^{-4}\,\mathrm{m/s}$, $\bar{C} = 2.3124\,\mathrm{kg/m^3}$ and $n = 3.8699$, whereas the following parameters were chosen without reference to any data: $\alpha = 0.1\,\mathrm{m^2/s^2}$, $C_{\mathrm{crit}} = 8\,\mathrm{kg/m^3}$ and $C_{\max} = 30\,\mathrm{kg/m^3}$. The reason for the second constant term of $v_{\mathrm{h}}(C)$ is only to define this function to be zero at a high concentration $C_{\max}$. This is essential when compression is set to zero and

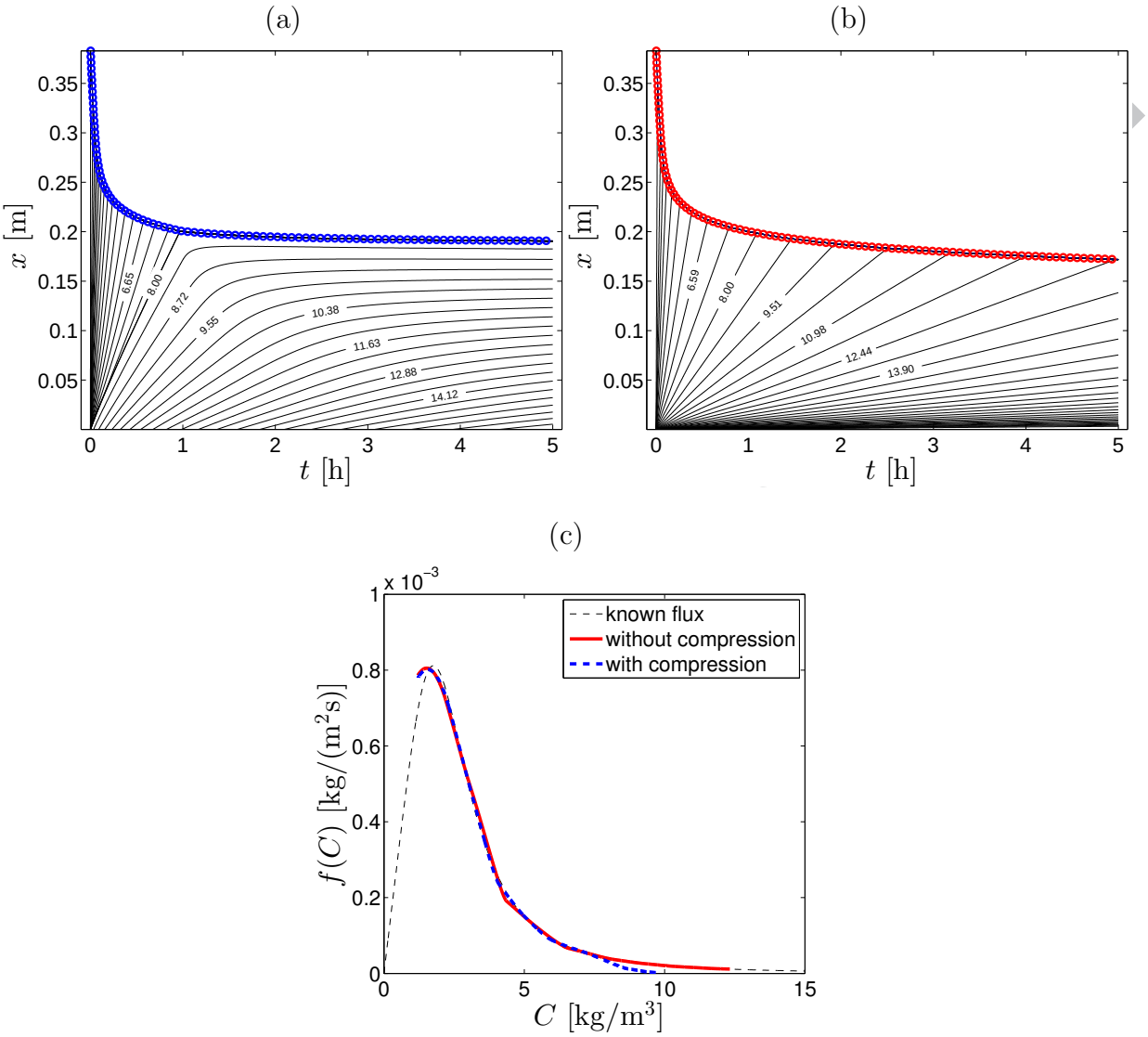

Figure 2: The estimation method applied to synthetic data obtained by numerical simulations (a) with and (b) without compression in the model. Plots (a) and (b) show iso-concentration lines (black, marked with concentrations) of the simulations and markers (coloured circles) where the data points $(t_j\,,\,x_j\,)$ are selected. Plot (c) shows the estimated fluxes together with the known flux function.

a power-law function for $v_{\rm h}(C)$ is used, since the solution of the corresponding hyperbolic PDE will take the maximum value at the bottom of the vessel. This feature does not appear for numerical solutions with an exponential function like Vesilind's, since such a function decreases to zero very fast.

The result of the estimation method is shown in Figure 2. From the simulation with compression shown in Figure 2(a), 94 data points were selected along the SBL, and from the simulation without compression shown in Figure 2(b), 98 data points were selected. In step 2 of the estimation method, the fitted curves $x = h(t)$ consist in both cases of 19 piecewise cubic polynomials. In Figure 2(a), the critical concentration $C_{\text{crit}} = 8$ kg/m^3 can be traced as the rightmost straight line joining the origin and the SBL at time $t \approx 1$ h. To the right of this straight line (and below the SBL) compression occurs, which can be seen from the curved iso-concentration contours.

Plot (c) shows the anticipated result that the estimated flux in the case of no compres-sion is the more accurate one. The estimated flux when taking compression into account deviates from the true flux for concentrations over 7.5 kg/m^3, which is slightly less than $C_{\text{crit}} = 8$ kg/m^3. An important observation is that the estimated flux function tends to zero already at about 10 kg/m^3, which is much lower than the true $C_{\text{max}} = 30$ kg/m^3. Moreover, for low concentrations, the deviations between the true and the estimated fluxes demon-strate the sensitivity of the method for these concentrations. One possible reason for this phenomenon is that the entire part of the estimated flux function for concentrations below 5 kg/m^3 corresponds to a small time interval in the beginning of the $x = h(t)$ curve, where it is descending fast.

4. Estimation using experimental data

Activated sludge was collected from the wastewater treatment plant in V¨aster˚as, Sweden. The plant treats sewage from a population equivalent to 118,000. The treatment process involves screening, pre-precipitation with iron sulphite, and biological treatment of the raw municipal wastewater. Four batch tests were conducted in a 1-litre full conical vessel with a vertex at the bottom, i.e., the horizontal cross-sectional area is zero at the bottom. The height is $H = 383$ mm and the top diameter 100 mm. The raw data of the samples are shown in Table 1.

Figure 3(a) contains the data points (red circles) of the SBL of Experiment 1 together with the fitted curve $x = h(t)$ (blue), which consists of 6 cubic polynomials. The coefficients

Table 1: Data of the sampled sludge. Each experiment was made in two replicas (a and b) and the initial concentraiton C_0 was chosen as the average of the two samples.

Exp.	Dilution (%)	Filtration paper (g)	Total mass (g)	Sample (g)	Sample (ml)	Conc. (g/m^3)	C_0 (aver.) (g/m^3)
1a	48.8	0.0888	0.1008	0.0120	10.0	1200	1230
1b	48.8	0.0905	0.1031	0.0126	10.0	1260	
2a	39.0	0.0897	0.1001	0.0104	10.0	1040	1045
2b	39.0	0.0885	0.0990	0.0105	10.0	1050	
3a	29.3	0.0920	0.0976	0.0056	10.0	560	570
3b	29.3	0.0900	0.0958	0.0058	10.0	580	
4a	19.5	0.0900	0.0945	0.0045	10.0	450	388
4b	19.5	0.0895	0.0927	0.0032	9.8	327	

of these polynomials are given in Table 2 and are obtained as the solution of a nonlinear least-squares problem with constraints that require the function $h(t)$ to be twice contin-uously differentiable, see Appendix AppendixA. According to the theory, the estimated flux function is then (only) continuously differentiable. Since a cubic polynomial has four coefficients, at least four data points in each time interval are needed. Figure 3(b) shows the estimated flux function (blue) and its complemented parts (dashed) for low and high concentrations; see step 3 of the estimation method. The straight line for high concentra-tions has been drawn from the last point on the blue flux curve to the chosen maximum concentration $C_{\max} = 30$ kg/m^3. The flux function in (b) was then used for the simulation of the four batch tests shown in plots (c)–(f) together with the data points of the respective experiment.

The similar procedure was carried out for Experiment 4 (Figure 4). (We do not provide the coefficients of all cubic polynomials that make up the fitted $h(t)$.) Naturally, the best agreement between simulation and data is obtained for the experiment that was used for the estimation; see Figure 3(c) for Experiment 1 and Figure 4(f) for Experiment 4. The reproductions of the other data sets were also found to be acceptable.

Table 2: Polynomial coefficients of the fitted curve $h(t) = a_j t^3 + b_j t^2 + c_j t + d_j$, $t \in I_j$, where I_j is time subinterval $j = 1, \ldots, 6$, for Experiment 1; see Figure 3(a).

Interval no. j	Subinterval I_j [h]	a_j [m/h^3]	b_j [m/h^2]	c_j [m/h]	d_j [m]
1	[0, 0.06666]	-0.000000	10.690564	-2.432308	0.393941
2	[0.06666, 0.13333]	-48.423468	20.375258	-3.077954	0.408289
3	[0.13333, 0.2]	-2.961595	2.190508	-0.653321	0.300528
4	[0.2, 0.26666]	-1.481030	1.302169	-0.475653	0.288683
5	[0.26666, 1.0]	-0.052430	0.159289	-0.17088	0.261593
6	[1.0, 5.0]	-0.000157	0.002470	-0.014066	0.209319

We have earlier promised that $h \in C^2$ implies an estimated flux $f \in C^1$, i.e., there should be no cusps along the graph of f. That this is indeed the case also for the graph of f in Figure 4(b) can be seen in Figure 5, which shows a zoomed view near the concentration $C = 4.8$ kg/m^3.

In Figure 6, the estimated fluxes from the four experiments are shown together with a nonlinear least-squares fit of the Vesilind hindered-settling velocity $v_0 \mathrm{e}^{-r_\mathrm{v} C}$ as well as that of Diehl (3). If C_max in (3) is used as a parameter in the least-squares fit, together with v_0, C^- and n, then the value $C_\mathrm{max} \approx 12$ kg/m^3 is obtained. This is in agreement with the synthetic test where compression was used in the model; see Figure 2(c), which shows that the estimated flux erroneously becomes zero at a too low concentration. Since we expect some compression in the real data, we choose a large fixed value of $C_\mathrm{max} = 30$ kg/m^3 before the nonlinear fit was obtained with the remaining three parameters (v_0, C^- and n).

The two flux functions were then used for the simulation and comparison of the four expriments (Figures 7 and 8).

5. Discussion and conclusions

A newly developed method for estimating a large part of the hindered-settling flux function has been validated with synthetic and experimental data. The input data are measurements of the descending SBL during a single batch sedimentation test in a conical vessel

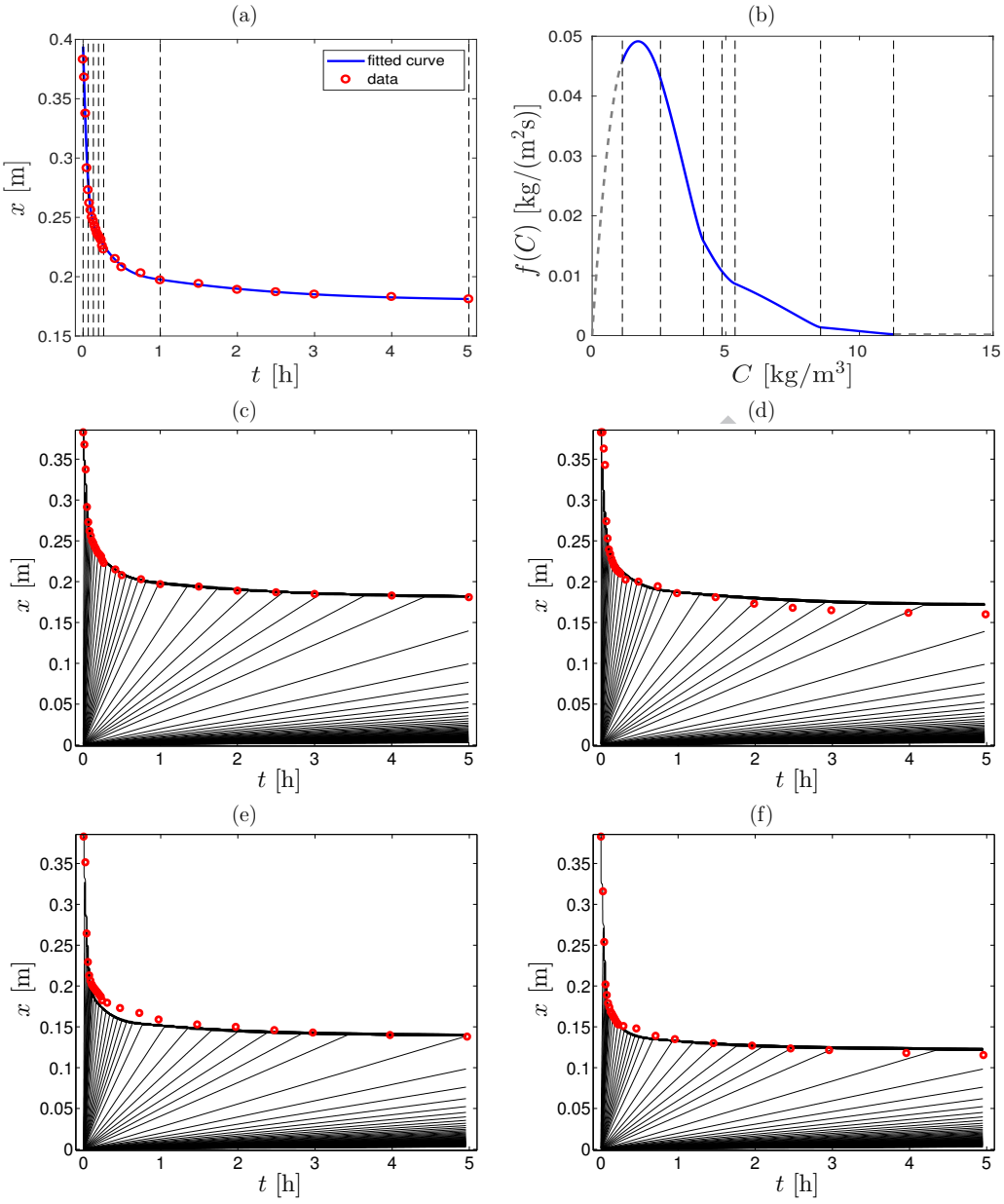

Figure 3: Experiment 1: (a) Height data of the SBL and fitted curve $x = h(t)$. The vertical dashed lines show the division of the time subintervals I_j, $j = 1, \ldots, 6$, in which $h(t)$ equals a cubic polynomial; cf. Table 2. (b) Identified flux function. (c)–(f) Simulation results using the estimated flux compared with data of the four experiments: (c) $C_0 = 1.230\,\mathrm{kg/m^3}$ (d) $C_0 = 1.045\,\mathrm{kg/m^3}$, (e) $C_0 = 0.570\,\mathrm{kg/m^3}$ and (f) $C_0 = 0.388\,\mathrm{kg/m^3}$.

in which the suspension occupies a perfect cone with its vertex at the bottom. Another advantage of the estimation method is that no advanced equipment is needed. The method

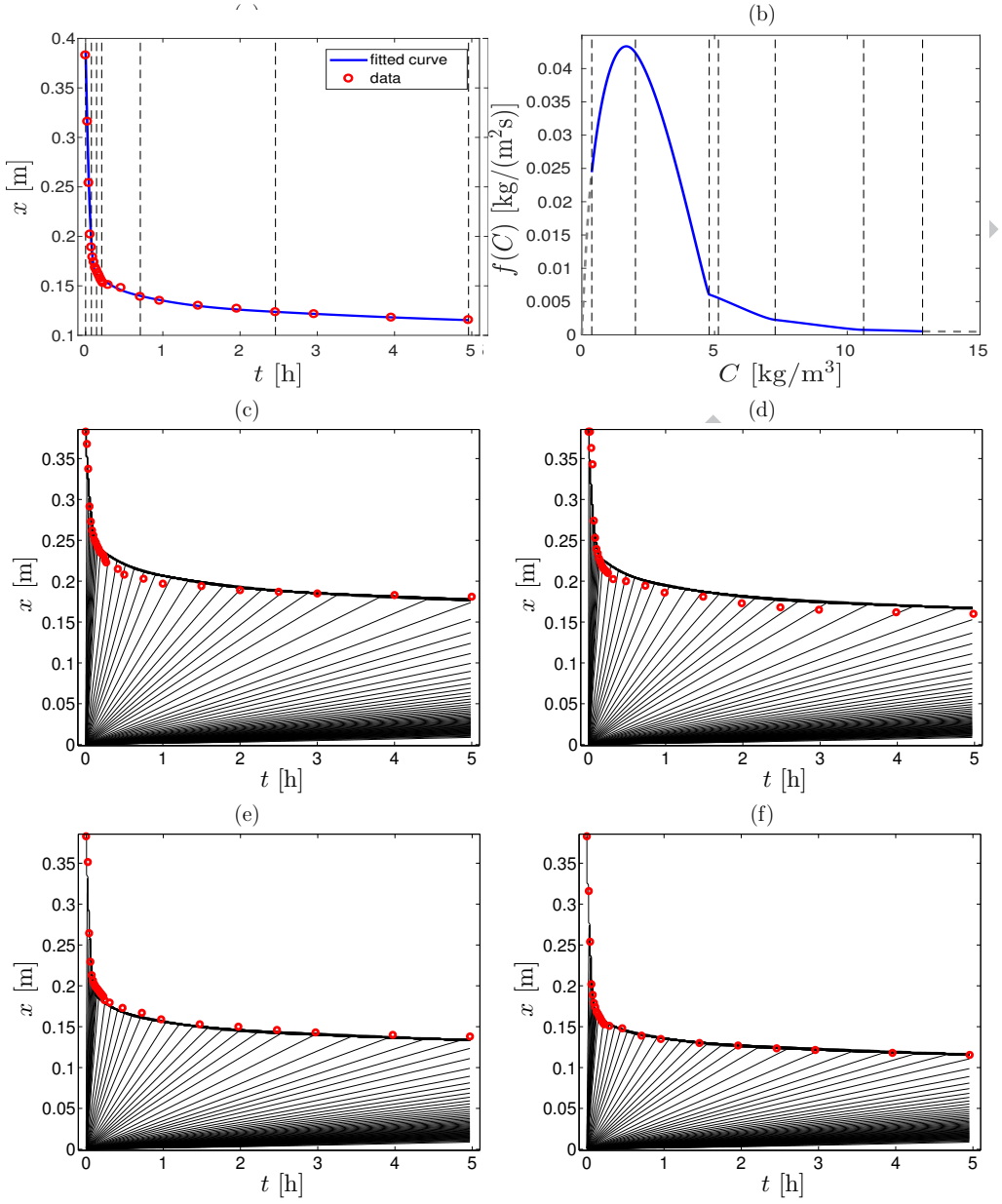

Figure 4: Experiment 4: (a) Height data of the SBL and fitted curve $x = h(t)$. The vertical dashed lines show the division of the time subintervals I_j, $j = 1, \ldots, 6$, in which $h(t)$ equals a cubic polynomial. (b) Identified flux function. (c)–(f) Simulation results using the estimated flux compared with data of the four experiments: (c) $C_0 = 1.230\,\mathrm{kg/m^3}$ (d) $C_0 = 1.045\,\mathrm{kg/m^3}$, (e) $C_0 = 0.570\,\mathrm{kg/m^3}$ and (f) $C_0 = 0.388\,\mathrm{kg/m^3}$.

has been developed for ideal suspensions that exhibit no compressive behaviour and can therefore only be used to estimate the flux function for concentrations below the critical

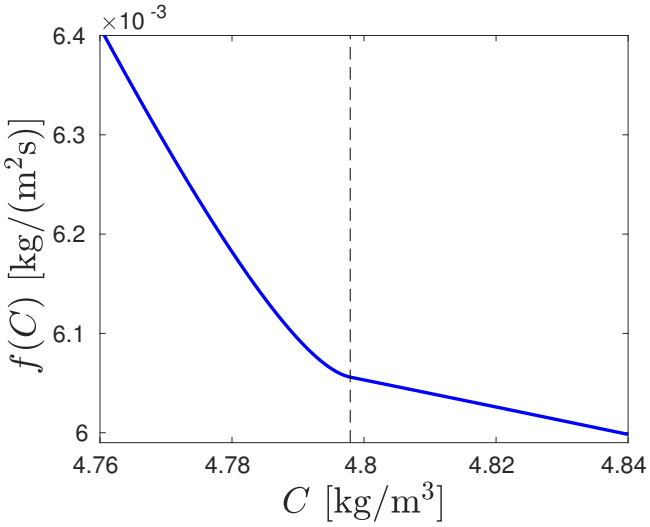

Figure 5: Zoom of the continuously differentiable flux function $f(C)$ of Figure 4(b).

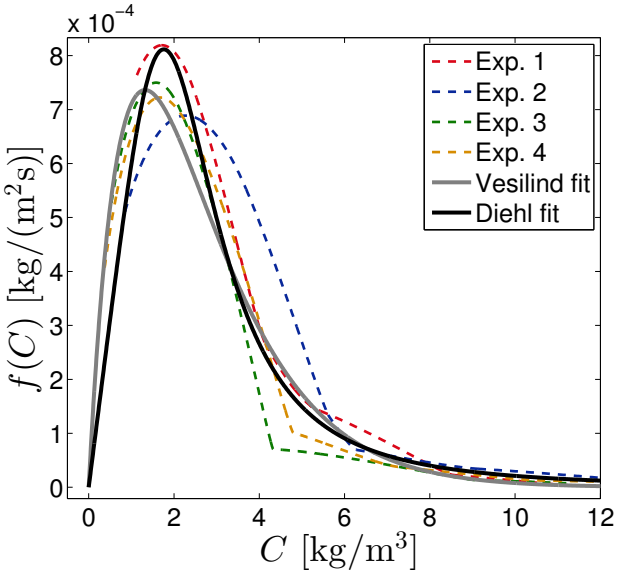

Figure 6: Estimated fluxes from Experiments 1–4 and fitted to these four are two parametrized flux functions (Vesilind and Diehl). The resulting parameters are for the Diehl flux (where $C_{\max} = 30$ kg/m^3 is set beforehand): $v_0 = 6.2153 \times 10^{-4}$ m/s, $C \equiv 2.3124$ kg/m^3, $n = 3.8699$, and for the Vesilind flux: $v_0 = 1.5129 \times 10^{-3}$ m/s, $r_{\mathrm{V}} = 0.7559$ m^3/kg.

concentration where hindered settling is the dominant process. The initial short time period, where the concentration increases rapidly just below the SBL, corresponds to a large part of the flux that is estimated. Hence, the method is sensitive to measurement errors,

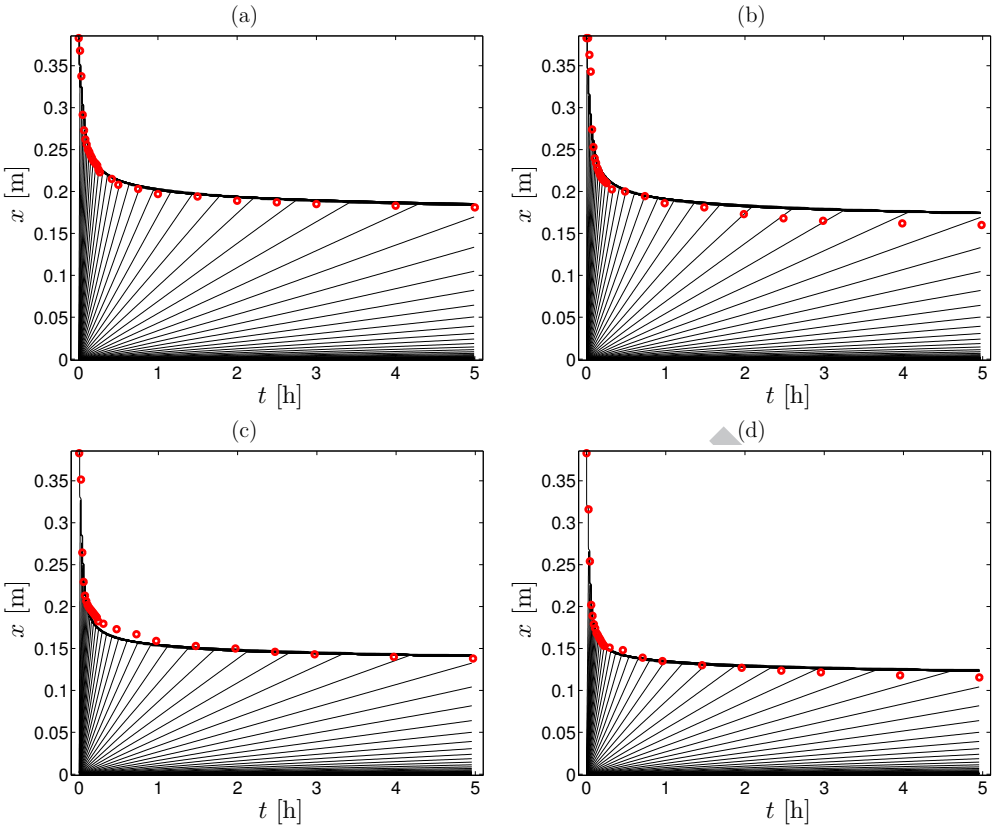

Figure 7: Simulations (black) with the Vesilind flux function compared to the data (red) of Experiments 1–4 shown in (a)–(d), respectively.

in particular, at the beginning of an experiment. This is confirmed by the examples using synthetic data, which can be seen as ideal: there is not a complete agreement between the estimated flux and known flux for low concentrations (Figure 2(c)).

Furthermore, it is very difficult to start a batch experiment with a homogeneous suspension where all particles are at rest at time $t = 0$. The stirring before the start causes an induction period, during which time other phenomena may also occur, such as flocculation. Induction periods in data from batch tests in cylindrical vessels can be averted via transformation (Diehl, 2015); however, it is not obvious how to do this when the cross-sectional area varies with the height. Induction periods were also present in the reported experiments. The length of the induction period increases with the initial concentration. Other well-known sources of non-ideal one-dimensional behaviour are attributed to polydispersivity and wall

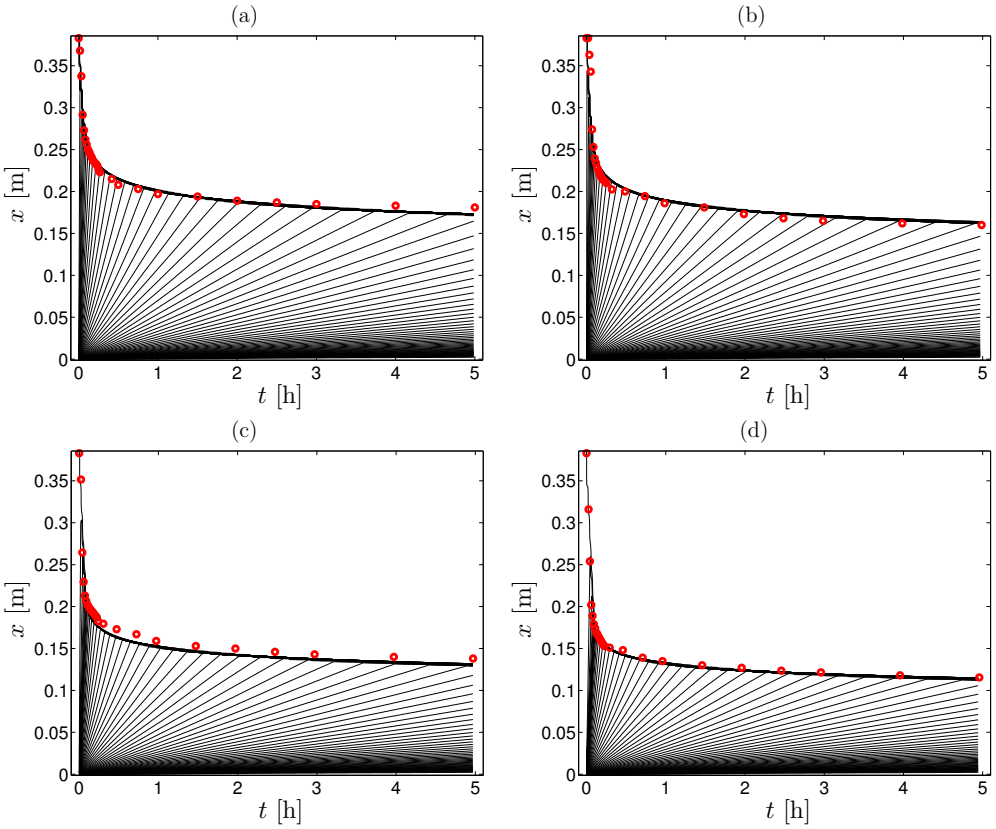

Figure 8: Simulations (black) with the Diehl flux function compared to the data (red) of Experiments 1–4 shown in (a)–(d), respectively.

effects. The experiments showed a prominent concave meniscus up to 0.7 mm in height from the floor of the interface.

Despite these theoretical and experimental inherent difficulties, straightforward use of the estimation method gave promising results. The method needs however to be developed further both theoretically and experimentally. One theoretically-based recommendation would be to obtain an estimated flux with higher regularity and with only one inflection point. Before this is done, and as we have presented here (step 4 of the estimation method), a final fit with a standard nonlinear least-squares method can be performed to obtain parameters of either the exponential Vesilind flux function or a power-law function. Simulations with both fluxes reproduced the experiments satisfactorily, with the power-law function being in slight favour, which is in agreement with the findings by Torfs et al. (2017).

Acknowledgements

RB and JC are supported by BASAL project CMM, Universidad de Chile and Centro de Investigaci´on en Ingenier´ıa Matem´atica (CI²MA), Universidad de Concepci´on. In addition RB is supported by Fondecyt project 1170473; Fondef project ID15I10291, and project CONICYT/FONDAP/15130015.

AppendixA. Fitting piecewise cubic polynomials to data

The given N pairs of data points representing the SBL $x = h(t)$, $0 \leqslant t \leqslant t_N$, are indexed as follows:

$$(t_j, x_j), \qquad j = 1, \ldots, j_2, \ldots, j_3, \ldots, j_n, \ldots, N. \tag{A.1}$$

Let $j_1 := 1$ and $j_{n+1} := N$. Then the cubic polynomial no. i is fitted to the data points j_i, . . . , $j_{i+1} - 1$ (and the additional last point no. N for the last subinterval no. n). We want to fit smooth functions $h_i(t)$ that together make up the function $h(t)$ in the following way:

$$h(t) = h_i(t) = a_i t^3 + b_i t^2 + c_i t + d_i \qquad t_{j_i} < t \leqslant t_{j_{i+1}}, \quad i = 1, \ldots, n, \tag{A.2}$$

At the fitting points, we impose the continuity constraints

$$h_{i-1}(t_{j_i}) = h_i(t_{j_i}), \quad i = 2, \ldots, n, \tag{A.3}$$

$$h'_{i-1}(t_{j_i}) = h'_i(t_{j_i}), \quad i = 2, \ldots, n, \tag{A.4}$$

$$h''_{i-1}(t_{j_i}) = h''_i(t_{j_i}), \quad i = 2, \ldots, n. \tag{A.5}$$

In order to obtain a decreasing and convex $h(t)$, it is sufficient to impose the following constraints (Bürger and Diehl, 2013):

$$a_i < 0, \quad b_i > 0, \quad i = 1, ..., n \tag{A.6}$$

$$h'_n(t_N) = 3a_n t_N^2 + 2b_n t_N + c_n < 0, \tag{A.7}$$

$$h''_n(t_N) = 6a_n t_N + 2b_n > 0. \tag{A.8}$$

Let $\boldsymbol{p}_i = (a_i, b_i, c_i, d_i)^{\mathrm{T}}$ and $\boldsymbol{q}(t) = (t^3, t^2, t, 1)^{\mathrm{T}}$, such that $h_i(t) = \boldsymbol{p}_i^{\mathrm{T}}\boldsymbol{q}(t)$, and define the vectors and matrices

$$\boldsymbol{p} := \begin{pmatrix} \boldsymbol{p}_1 \\ \boldsymbol{p}_2 \\ \vdots \\ \boldsymbol{p}_n \end{pmatrix}, \quad \boldsymbol{x}_i := \begin{pmatrix} x_{j_i} \\ x_{j_i+1} \\ \vdots \\ x_{j_{i+1}-1} \end{pmatrix}, \quad \boldsymbol{x} = \begin{pmatrix} \boldsymbol{x}_1 \\ \vdots \\ \boldsymbol{x}_n \\ x_N \end{pmatrix},$$

$$\boldsymbol{Q}_i = \begin{pmatrix} \boldsymbol{q}(t_{j_i})^{\mathrm{T}} \\ \boldsymbol{q}(t_{j_i+1})^{\mathrm{T}} \\ \vdots \\ \boldsymbol{q}(t_{j_{i+1}-1})^{\mathrm{T}} \end{pmatrix}, \quad \boldsymbol{Q} = \begin{pmatrix} \boldsymbol{Q}_1 & & \boldsymbol{0} \\ & \ddots & \\ \boldsymbol{0} & & \boldsymbol{Q}_n \\ \boldsymbol{0} & & \boldsymbol{q}(t_N)^{\mathrm{T}} \end{pmatrix}.$$

The equality constraints (A.3)–(A.5) can be written $\boldsymbol{R}\boldsymbol{p} = \boldsymbol{0}$ by means of the matrices

$$\boldsymbol{R}_i = \Big(\boldsymbol{q}(t_{j_i}),\ \boldsymbol{q}'(t_{j_i}),\ \boldsymbol{q}''(t_{j_i})\Big)^{\mathrm{T}},$$

$$\boldsymbol{R} = \begin{pmatrix} \boldsymbol{R}_2 & -\boldsymbol{R}_2 & & \boldsymbol{0} \\ & \ddots & \ddots & \\ \boldsymbol{0} & & \boldsymbol{R}_n & -\boldsymbol{R}_n \end{pmatrix}.$$

For the inequality constraints, we let $\varepsilon > 0$ be a small number and $\boldsymbol{1}_{m\times n}$ denote an $m \times n$ matrix full of ones. We define $\boldsymbol{e}_1 = (1,\ 0,\ 0,\ 0)^{\mathrm{T}}$, $\boldsymbol{e}_2 = (0,\ 1,\ 0,\ 0)^{\mathrm{T}}$, denote by $\boldsymbol{I}_n$ the $n \times n$ identity matrix, and define

$$\boldsymbol{M} = \begin{pmatrix} \boldsymbol{I}_n \otimes \boldsymbol{e}_1^{\mathrm{T}} \\ -\boldsymbol{I}_n \otimes \boldsymbol{e}_2^{\mathrm{T}} \\ \Big(\boldsymbol{0}_{1\times 4(n-1)} \quad \boldsymbol{q}'(t_N)^{\mathrm{T}}\Big) \\ \Big(\boldsymbol{0}_{1\times 4(n-1)} \quad -\boldsymbol{q}''(t_N)^{\mathrm{T}}\Big) \end{pmatrix},$$

$$\boldsymbol{b} = -\varepsilon \Big(\boldsymbol{1}_{2n\times 1}^{\mathrm{T}},\ 0,\ 0\Big)^{\mathrm{T}}.$$

Then the inequality constraints $\boldsymbol{M}\boldsymbol{p} \leqslant \boldsymbol{b}$ imply (A.6)–(A.8). The parameters $\boldsymbol{p}$ are determined by the quadratic programming problem

$$\text{minimize} \quad J(\boldsymbol{p}) = (\boldsymbol{Q}\boldsymbol{p} - \boldsymbol{z})^{\mathrm{T}}(\boldsymbol{Q}\boldsymbol{p} - \boldsymbol{z})$$

$$\text{subject to} \quad \boldsymbol{Rp} = \boldsymbol{0}, \quad \boldsymbol{Mp} \leqslant \boldsymbol{b}.$$

This problem has a unique solution (Bürger and Diehl, 2013).

Anestis, G., 1981. Eine eindimensionale Theorie der Sedimentation in Absetzbehältern veränderlichen Querschnitts und in Zentrifugen. Ph.D. thesis, TU Vienna, Austria.

Burger, R., Careaga, J., Diehl, S., 2017a. Entropy solutions of a scalar conservation law modeling sedimentation in vessels with varying cross-sectional area. SIAM J. Appl. Math. 77 (2), 789–811.

Burger, R., Careaga, J., Diehl, S., 2017b. A simulation model for settling tanks with varying cross-sectional area. Chem. Eng. Commun. 204 (11), 1270–1281.

Burger, R., Careaga, J., Diehl, S., 2018. Flux identification of scalar conservation laws from sedimentation in a cone. IMA J. Appl. Math. 83 (3), 526–552.

Burger, R., Diehl, S., 2013. Convexity-preserving flux identification for scalar conservation laws modelling sedimentation. Inverse Problems 29 (4), 045008.

Burger, R., Diehl, S., Nopens, I., 2011. A consistent modelling methodology for secondary settling tanks in wastewater treatment. Water Res. 45 (6), 2247–2260.

De Clercq, J., Jacobs, F., Kinnear, D. J., Nopens, I., Dierckx, R. A., Defrancq, J., Vanrolleghem, P. A., 2005. Detailed spatio-temporal solids concentration profiling during batch settling of activated sludge using a radiotracer. Water Res. 39, 2125–2135.

Derlon, N., Thu¨rlimann, C., Du¨rrenmatt, D., Villez, K., 2017. Batch settling curve registration via image data modeling. Water Res. 114, 327–337.

Diehl, S., 2007. Estimation of the batch-settling flux function for an ideal suspension from only two experiments. Chem. Eng. Sci. 62, 4589–4601.

Diehl, S., 2015. Numerical identification of constitutive functions in scalar nonlinear convection–diffusion equations with application to batch sedimentation. Appl. Num. Math. 95, 154–172.

François, P., Locatelli, F., Laurent, J., Bekkour, K., 2016. Experimental study of activated sludge batch settling velocity profile. Flow Measurement and Instrumentation 48, 112–117.

Grassia, P., Usher, S. P., Scales, P. J., 2011. Closed-form solutions for batch settling height from model settling flux functions. Chem. Eng. Sci. 66 (5), 964–972.

Iritani, E., Hashimoto, T., Katagiri, N., 2009. Gravity consolidation-sedimentation behaviors of concentrated TiO_2 suspension. Chem. Eng. Sci. 64 (21), 4414–4423.

Kynch, G. J., 1952. A theory of sedimentation. Trans. Faraday Soc. 48, 166–176.

Locatelli, F., François, P., Laurent, J., Lawniczak, F., Dufresne, M., Vazquez, J., Bekkour, K., 2015. Detailed velocity and concentration profiles measurement during activated sludge batch settling using an ultrasonic transducer. Sep. Sci. Tech. 50 (7), 1059–1065.

Mancell-Egala, W. A. S. K., Kinnear, D. J., Jones, K. L., Clippeleir, H. D., Takács, I., Murthy, S. N., 2016. Limit of stokesian settling concentration characterizes sludge settling velocity. Water Res. 90, 100–110.

Ozinsky, A. E., Ekama, G. A., 1995. Secondary settling tank modeling and design part 2: Linking sludge settleability measures. Water SA 21 (4), 333–349.

Ramin, E., W´agner, D. S., Yde, L., Binning, P. J., Rasmussen, M. R., Mikkelsen, P. S., Pl´osz, B. G., 2014. A new settling velocity model to describe secondary sedimentation. Water Res. 66, 447–458.

Takacs, I., Patry, G. G., Nolasco, D., 1991. A dynamic model of the clarification-thickening p rocess. Water Res. 25 (10), 1263–1271.

Torfs, E., Balemans, S., Locatelli, F., Diehl, S., Burger, R., Laurent, J., Fran¸cois, P., Nopens, I., 2017. Onconstitutive functions for hindered settling velocity in 1-d settler models: Selection of appropriate model structure. Water Res. 110, 38–47.

Torfs, E., Mart´ı, M. C., Locatelli, F., Balemans, S., Bu¨rger, R., Diehl, S., Laurent, J., Vanrolleghem, P. A., Franc¸ois, P., Nopens, I., 2016a. Concentration-driven models revisited: towards a unified framework to model settling tanks in water resource recovery facilities. Water Sci. Tech. 75 (3), 539–551.

Torfs, E., Nopens, I., Winkler, M., Vanrolleghem, P., Balemans, S., Smets, I., 2016b. Settling tests. IWA publisher, Ch. 6, pp. 235–262.

Vanderhasselt, A., Vanrolleghem, P. A., 2000. Estimation of sludge sedimentation parameters from single batch settling curves. Water Res. 34 (2), 395–406.

Vesilind, P. A., 1968. Design of prototype thickeners from batch settling tests. Water Sewage Works 115 (7), 302–307.

White, D. A., Verdone, N., 2000. Numerical modelling of sedimentation processes. Chem. Eng. Sci. 55, 2213–2222.

Zeidan, A., Rohani, S., Bassi, A., 2003. Review and comparison of solids settling velocity models. Reviews in Chemical Engineering 19, 473–530.

Zhang, D., Li, Z., Lu, P., Zhang, T., Xu, D., 2006. A method for characterizing the complete settling process of activated sludge. Water Res. 40, 2637–2644.

Novel method related to inverse problem of partial differential equation tested.

Inputs are data of sludge blanket level of one batch settling test in a cone.

Output is a large portion of the hindered-settling flux, or equivalently, velocity.